

Magnetic anisotropy and magnetoelastic  
property for magnetic Weyl semimetallic

Co<sub>2</sub>MnGa thin films

Magnetic anisotropy and magnetoelastic  
properties of Weyl magnetic semimetal

Co<sub>2</sub>MnGa thin films

[O. Chumak](#)<sup>1</sup>, [A. Nabałek](#)<sup>1,\*</sup>, [L.T. Baczewski](#)<sup>1</sup>, [T. Seki](#)<sup>2</sup>, [J. Wang](#)<sup>2,3</sup>, K. Takanashi<sup>2,4</sup> and [H. Szymczak](#)<sup>1</sup>

<sup>1</sup>Institute of Physics PAS, Al. Lotników 32/46, 02-668 Warsaw, Poland

<sup>2</sup>Institute for Materials Research, Tohoku University, 980-8577, Miyagi Japan

<sup>3</sup>Innovative Functional Materials Research Institute, National Institute of Advanced Industrial Science and Technology, 463-8560, Aichi, Japan

<sup>4</sup>Advanced Science Research Center, Japan Atomic Energy Agency, 319-1195, Ibaraki, Japan

**ABSTRACT.** The magnetic anisotropy and magnetoelastic properties of the magnetic Weyl semimetal  $\text{Co}_2\text{MnGa}$  were investigated by exploiting the  $\text{Co}_2\text{MnGa}$  thin films with different chemical orderings. The epitaxial layers were grown by sputtering directly on  $\text{MgO}$  (001) and the annealing temperatures after the deposition were varied, which allowed us to change the chemical ordering of  $\text{Co}_2\text{MnGa}$ . We observed a clear relationship between the annealing temperature and the parameters of magnetic property. The most significant changes of both the magnetic anisotropy and the magnetoelastic properties were correlated with the appearance of the  $L2_1$  ordered phase, suggesting that the emergence of magnetic Weyl semimetallic feature is the key point to vary these magnetic properties.

## I. INTRODUCTION.

Some full Heusler alloys of the  $X_2YZ$  type (where  $X$  and  $Y$  are transition metals) have been theoretically predicted to exhibit ferromagnetic Weyl semimetal properties [1,2]. Among them, Weyl semimetallic feature has been experimentally confirmed in bulk single crystals of  $\text{Co}_2\text{MnGa}$  (CMG) through the detection of linear band dispersions using photoemission spectroscopy [3]. Epitaxial thin films of a CMG Heusler alloy with topological properties have gained significant attention due to their potential applications in spintronics and spin-caloritronics since the CMG films exhibit the large anomalous Hall effect (AHE) and anomalous Nernst effect (ANE) [4,5,6]. Considering the potential use of AHE and ANE in future technologies, e.g. as a flexible device [6], understanding the magnetic anisotropy and magnetoelastic properties of these films is crucial for optimizing their performance in practical applications.

The Co-based full Heusler alloys exhibit different phases: the  $L2_1$  phase with a perfectly ordered atomic arrangement, the B2 phase with  $Y-Z$  atom displacements, the  $D0_3$  phase with  $\text{Co}-Y$  displacements, or the A2 phase where the Co, Y, and Z elements are randomly distributed [7]. According to the previous work [8,9], the degree of chemical ordering in the  $L2_1$  structure of CMG is related to the emergence of magnetic Weyl semimetallic feature and also plays a key role in determining its magnetic properties [10] including the direction of easy magnetization and the magnitude of magnetocrystalline anisotropy (MCA). The electronic structure is varied by the chemical ordering, leading to changes in magnetic interactions and strain-induced effects. Studying these properties in thin films with different degrees of chemical ordering can provide insight into how structural factors influence magnetism at the atomic level. This is particularly relevant for improving the stability and tunability of magnetic anisotropy, which are essential for sensor technologies, memory devices, and spintronic applications.

The previous work [11] reported the effect of disorder and vacancy defects on the electrical transport

properties of CMG thin films. It was shown that by the application of different annealing temperatures, the long-range degree of chemical ordering was changed from A2 to B2 plus  $L2_1$  upon annealing at  $500^\circ\text{C}$  or above. Also, a remarkable strain-induced MCA was reported for the epitaxial CMG films [12], and the magnitudes of both perpendicular to the plane and in-plane MCA increase with the layer distortion [13], which suggests the magnetoelastic effect to be significant.

In this paper, we focus on the correlation between the chemical ordering and MCA and magnetoelastic properties of the epitaxial CMG thin films. Since our previous results show that magnetoelastic properties of the epitaxial  $\text{Co}_2(\text{Fe,Mn})\text{Si}$  Heusler alloy thin films are strongly anisotropic [14] and the strain influenced on the magnitude of MCA [15], the present results for the CMG are compared with the previous results for the other Heusler alloy thin films.

## II. EXPERIMENT

The 75 nm thick epitaxial  $\text{Co}_2\text{MnGa}$  layers were grown directly on  $\text{MgO}$  (001) and protected by 2 nm Al cap layers. After deposition, the samples were annealed at different temperatures in the range from  $300^\circ\text{C}$  to  $500^\circ\text{C}$  in vacuum for 3 hours. We present here the results for  $\text{Co}_2\text{MnGa}$  samples annealed at  $300^\circ\text{C}$ ,  $400^\circ\text{C}$  and  $500^\circ\text{C}$ . The details of samples preparation were described in the previous paper [11], in which the structural studies were carried out using transmission electron microscopy (TEM), energy-dispersive x-ray (EDX) analysis, x-ray diffraction (XRD) analysis as well as positron annihilation measurements.

The measurement of anisotropic magnetoelastic properties of the CMG thin films was performed using the strain modulated ferromagnetic resonance (SMFMR) technique [16, 17]. It is one of the methods that allows the study of anisotropic magnetoelastic properties of thin films, while the conventional ferromagnetic resonance (FMR) technique is a method to accurately determine the magnetic anisotropy. Hence, the conventional FMR

technique was used to determine the magnetic anisotropy of the thin films.

In the FMR studies, we used X-band Bruker EMX EPR spectrometer. The maximum field attainable in this system was about 18 kOe. This system was used to study the angular dependencies of the resonance field in the in-plane and out-of-plane directions, which were used to calculate the cubic and uniaxial MCA constants perpendicular to the film plane, respectively.

The SMFMR studies were performed using an X-band Radiopan EPR spectrometer modified for this purpose, with a maximum field attainable of about 9.5 kOe. Hence, only the in-plane studies could be performed to determine the two magnetoelastic constants characteristic of the samples with cubic symmetry. The procedure to determine the magnetoelastic constants was the same as that described in our previous paper [14]. In the SMFMR technique, we compare the magnitudes of two FMR signals, one of which is modulated by AC (100 kHz) magnetic field and the other one by periodic (48 kHz) strain [14,16,17]. The comparison of these two signals enables the determination of the shift of the resonance line caused by the strain, and then, using an appropriate model, calculate the magnetoelastic constants.

The magnetization of the films was measured at room temperature using the vibrating sample magnetometer (VSM) in the magnetic field range of  $\pm 2$  kOe.

### III. RESULTS AND DISCUSSION

According to the previous paper [11], after annealing at 300°C only the A2 phase was detected. The annealing at 400°C dramatically increased the amount of the B2 phase (87%), and after annealing at 500°C the L2<sub>1</sub> phase (23%) in addition to the B2 phase appeared. The CMG films contained divacancies at a concentration of at least 100 ppm, and these were partially annealed out at a temperature above 400°C near the interface with MgO [11]. The results presented in Ref. [11] also showed that after increasing the annealing temperature up to 500°C both longitudinal and anomalous Hall conductivities were dramatically enhanced, although they remained lower than for the bulk materials.

The magnetization hysteresis loops of the three samples are shown in Fig. 1(a-c). They were measured in an external magnetic field with the range of  $\pm 2$  kOe, in which the magnetic field was applied

along the in-plane [100] axis or [110] axis of the CMG layer.

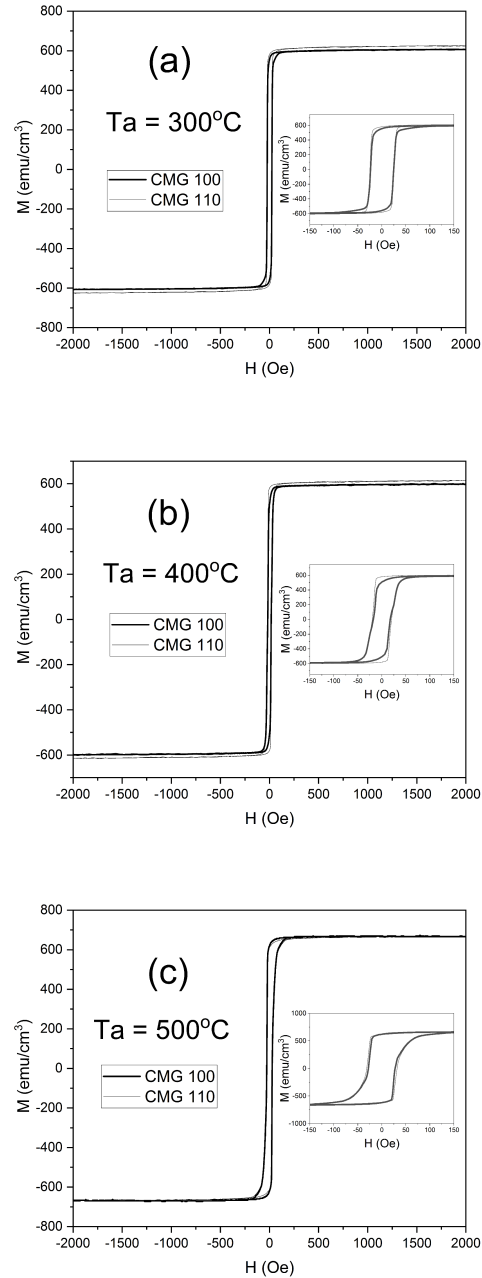


FIG 1. Magnetization hysteresis loops for the three samples. The samples were annealed at  $T_a = 300^\circ\text{C}$  (a),  $400^\circ\text{C}$  (b) and  $500^\circ\text{C}$  (c). The loops were measured at room temperature and the external magnetic field was applied in the in-plane direction parallel to the [100] axis or [110] axis of CMG. The insets show the enlarged hysteresis loops in the magnetization reorientation range of the magnetic field.

The saturation magnetization for this compound was theoretically estimated to be 4 Bohr magneton per formula unit [18]. If we assume the density of the magnetic layer to be 8.4 g/cm<sup>3</sup>, the theoretical saturation magnetization is about 780 emu/cm<sup>3</sup>. The values of saturation magnetization for all samples were lower than the theoretical value (see Fig. 1).

The saturation magnetization was found to be about 625 emu/cm<sup>3</sup>, 615 emu/cm<sup>3</sup>, and 660 emu/cm<sup>3</sup>, and the coercive field about 25 Oe, 20 Oe, and 30 Oe for Ta = 300°C, 400°C, and 500°C, respectively. Comparison of the in-plane hysteresis loops for the [100] and [110] crystallographic axis of CMG shows that the in-plane MCA is relatively weak, with an easy axis along the [100] direction for Ta= 300°C and 400°C. In the case of Ta = 500°C, it was difficult to determine the direction of the easy axis from the magnetization curves. For accurate determination of the MCA, the FMR studies were performed.

Fig. 2(a-c) shows the room temperature in-plane angular dependencies of the FMR resonance field ( $H_{rez}$ ) for the samples at Ta = 300°C (Fig. 2(a)), 400°C (Fig. 2(b)) and 500°C (Fig. 2(c)). For all the samples the [110] axis of CMG was parallel to the [100] (or equivalent) axis of the cubic MgO substrate. The angular dependence of the FMR resonance field reveals a four-fold symmetry characteristic (in this orientation) for the cubic epitaxial CMG layer. The easy axis of magnetization, corresponding to the minimum of  $H_{rez}$ , is parallel to the [110] axis of CMG for Ta=300°C and 400°C. However, for Ta = 500°C, it is changed and became parallel to the [100] axis of CMG.

Fig. 3 shows the room temperature angular dependencies of the out-of-plane FMR resonance field, for the three samples. The zero angle corresponds to the direction perpendicular to the film plane, and the 90-degree direction parallel to the [110] axis of CMG in-plane of the film. One can notice a slight increase of the resonance field in the perpendicular to the film orientation with increasing the annealing temperature, suggesting the changes of perpendicular MCA.

In Fig. 2 and Fig. 3, we present the resonance field for only the main (averaged or most intensive) lines observed in our experiments. In fact, the lines were split in many cases, revealing some fine structures most probably connected with the inhomogeneity of the sample. This effect was particularly visible in perpendicular orientation where the lines that constitute the fine structure were exceptionally

narrow. The effect of splitting disappeared in the in-plane orientation, where the typical widths of the FMR lines in the range from 50 Oe to 90 Oe were observed. In this paper, we will not discuss the effect of resonance lines splitting in more detail. In further analysis, we will only take into account the position of the main lines.

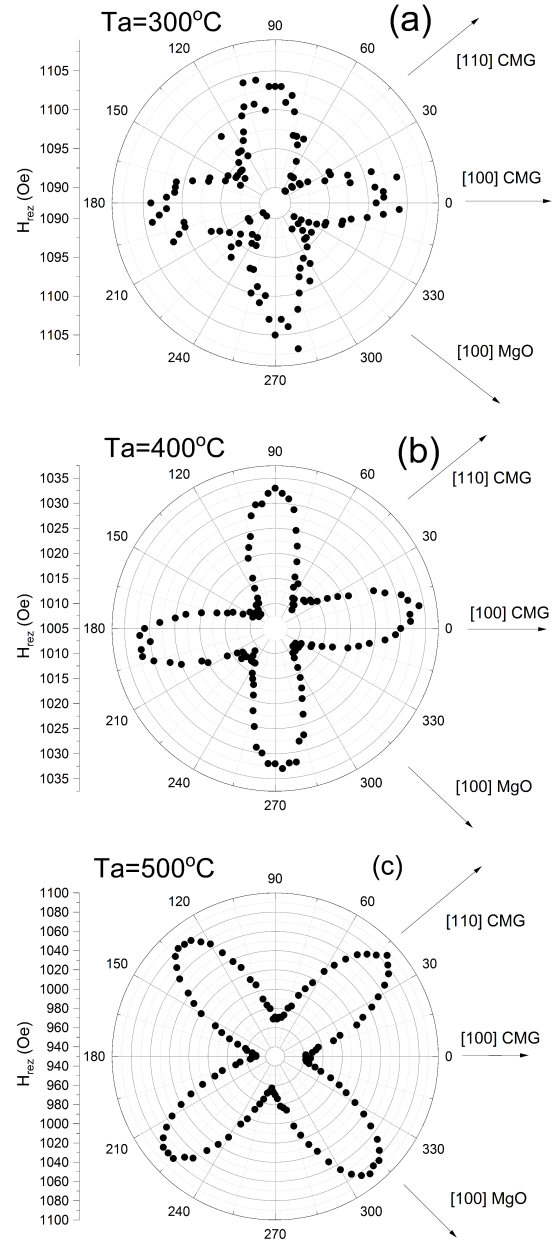


FIG 2. The room temperature angular dependencies of the in-plane FMR resonance field (X-band 9.37 GHz) for the three samples. The samples were annealed at Ta= 300°C (a), 400°C (b) and 500°C (c).

\*Contact author: nabia@ifpan.edu.pl

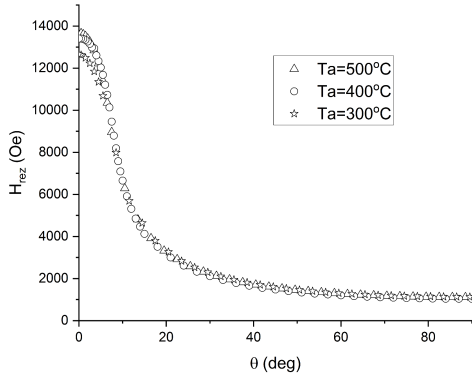


FIG 3. The room temperature angular dependencies of the out-of-plane FMR resonance field (X-band 9.37 GHz) for the three samples. The samples were annealed at  $T_a = 300^\circ\text{C}$  (stars),  $400^\circ\text{C}$  (circles), and  $500^\circ\text{C}$  (triangles).

In our analysis, we used the same model as that presented earlier in Ref. [14]. The magnetocrystalline energy was assumed to be described by the formula:

$$E_{mc} = K_p(1 - \alpha_3'^2) + K_1(\alpha_1'^2\alpha_2'^2 + \alpha_2'^2\alpha_3'^2 + \alpha_1'^2\alpha_3'^2), \quad (1)$$

where  $\alpha_i'$  are the directions cosines associated with the sample coordinate system, and the third coordinate is perpendicular to the film. The  $K_p$  and  $K_1$  are the perpendicular and the first cubic MCA constants, respectively. The anisotropy constants were calculated using the magnitudes of the resonance field measured along the [100], [110], and [001] direction (see Fig. 2 and Fig. 3) as well as the magnitudes of saturation magnetization. The applied model was presented in detail in our previous paper [14]. The results of the calculations are given in Table I.

TABLE I. The room temperature first cubic MCA constants,  $K_1$ , and the perpendicular MCA constant,  $K_p$ , for the samples annealed at the temperatures  $T_a$ .

$T_a$	$K_1$ ( $10^4$ erg/cm $^3$ )	$K_p$ ( $10^5$ erg/cm $^3$ )
300°C	-0.4	-4.5
400°C	-0.4	-7.4
500°C	2.2	-6.7

The change of the sign of  $K_1$  reflects the change of an easy axis of magnetization from [110] (negative value) to [100] (positive value). The negative sign of  $K_p$  means that the perpendicular MC energy adds to

the demagnetizing energy, making the in-plane orientation even more preferable.

The most significant change of  $K_1$  was observed after increasing the annealing temperature up to  $500^\circ\text{C}$ , which according to the structural analysis presented in Ref. [11] can be associated with the appearance of the  $L2_1$  phase. For the samples annealed at  $300^\circ\text{C}$  and  $400^\circ\text{C}$ ,  $K_1$  is about  $-0.4 \times 10^4$  erg/cm $^3$  and increases up to  $2.2$  erg/cm $^3$  for the sample annealed at  $500^\circ\text{C}$ . The magnitude of  $K_1$  of all samples is relatively low, i.e. of an order of  $10^4$  erg/cm $^3$ .

The perpendicular MCA constant for all investigated samples is negative of an order of  $10^5$  erg/cm $^3$ . The most remarkable change in  $K_p$  was after increasing the annealing temperature up to  $400^\circ\text{C}$ , i.e. with the appearance of the partially ordered B1 phase [11].

The results of the SMFMR studies are summarized in Table II.  $\Delta H_{100}$  and  $\Delta H_{110}$  are the shifts of the FMR resonance lines, measured in-plane of the film in the direction [100] and [110], respectively. These shifts were induced by the strains  $\epsilon_{11}$  and  $\epsilon_{22}$  of the quartz rod to which the samples were glued.  $\epsilon_{11}$  and  $\epsilon_{22}$  denote the strains in the direction perpendicular and parallel to the rod, respectively. As described in detail in Ref. [14], the strains were determined in each experiment using the calibration procedure to increase the accuracy of the magnetoelastic constants determination.

TABLE II. The shifts of the FMR lines measured using the SMFMR technique for the three samples, measured in the film plane with the external magnetic field applied parallel to the [100] axis ( $\Delta H_{100}$ ) or [110] axis ( $\Delta H_{110}$ ), caused by the periodic strains  $\epsilon_{11}$  and  $\epsilon_{22}$  of the polycrystalline quartz rod, to which the thin films were glued.

$T_a$	$\Delta H_{100}$ (Oe)	$\epsilon_{11}$ ( $10^{-6}$ )	$\epsilon_{22}$ ( $10^{-5}$ )	$\Delta H_{110}$ (Oe)	$\epsilon_{11}$ ( $10^{-6}$ )	$\epsilon_{22}$ ( $10^{-5}$ )
300°C	0.52	-2.2	1.80	0.77	-2.7	1.69
400°C	0.47	-2.9	1.47	0.37	-3.0	1.56
500°C	0.73	-3.0	1.56	-0.05	-2.6	1.63

The strains typically applied in our experiments ( $\epsilon_{11}$  about  $-3 \times 10^{-6}$  and  $\epsilon_{22}$  about  $1.5 \times 10^{-5}$ ) result in

\*Contact author: nabia@ifpan.edu.pl

shifts of the resonance lines of about 0.5 Oe. The difference between  $\Delta H_{100}$  and  $\Delta H_{110}$  reveals the anisotropy of the magnetoelastic effect. One can see that for Ta=300°C and 400°C this anisotropy is relatively weak, and for Ta=500°C very strong anisotropy of magnetoelastic properties was observed.

In our model (see Ref. [14] for details), we assumed the magnetoelastic energy of a cubic crystal to be described by two magnetoelastic constants  $b_1$  and  $b_2$  according to the formula [17]:

$$E_{me} = b_1(\alpha_1'^2 \varepsilon_{11}' + \alpha_2'^2 \varepsilon_{22}' + \alpha_3'^2 \varepsilon_{33}') + 2b_2(\alpha_1' \alpha_2' \varepsilon_{12}' + \alpha_2' \alpha_3' \varepsilon_{23}' + \alpha_1' \alpha_3' \varepsilon_{13}'), \quad (2)$$

where  $\alpha_i'$  and  $\varepsilon_{ij}'$  are direction cosines and strains in the coordinate system associated with the sample. The magnetoelastic constants, calculated in the framework of this model, are summarized in Table III.

TABLE III. Room temperature magnetoelastic  $b_1$  and  $b_2$  and magnetostriction  $\lambda_{100}$  and  $\lambda_{111}$  constants of the CMG films annealed at Ta 300°C, 400°C, and 500°C.

Ta	$b_1$ ( $10^7$ erg/cm $^3$ )	$b_2$ ( $10^7$ erg/cm $^3$ )	$\lambda_{100}$ ( $10^{-6}$ )	$\lambda_{111}$ ( $10^{-6}$ )
300°C	-0.92	-1.37	4.9	3.5
400°C	-0.91	-0.71	4.9	1.8
500°C	-1.43	-0.02	7.7	0.05

For isotropic samples  $b_1=b_2$ . Hence, the difference between magnetoelastic constants can be treated as a measure of the magnetoelastic properties anisotropy. As can be expected based on the results in Table II the largest difference between the  $b_1$  and  $b_2$  constants is for the sample annealed at 500°C. To calculate the  $b_1$  and  $b_2$  constants according to the model [14] the knowledge of the ratio of the elastic constants  $c_{12}/c_{11}$  is necessary. Unfortunately, there is quite a large discrepancy between the elastic constants presented in the literature. One review of the data available can be found in the paper [19]. In our calculations, we

used averaged values of all data presented in Ref. [19], i.e.  $c_{11}=281$  GPa,  $c_{12}=157$  GPa,  $c_{44}=132$  GPa. The knowledge of the elastic constants is also necessary to calculate the magnetostriction constants. The longitudinal magnetostriction constants for the [100] and [111] directions, i.e.  $\lambda_{100}$  and  $\lambda_{111}$  can be calculated using the formulas (3) [14]:

$$\lambda_{100} = -\frac{2b_1}{3(c_{11}-c_{12})}, \lambda_{111} = -\frac{b_2}{3c_{44}} \quad (3)$$

The calculated magnetostriction constants are also presented in Table III. However, they only refer to bulk materials. The actual magnetostriction, i.e. the changes of the sample dimensions in the external magnetic field, of the thin films is extremely small, because of the interaction of the thin magnetic film with a thick substrate. According to Eq. (3), the magnitudes of the magnetostriction constants are proportional to magnetoelastic constants and have opposite signs.

The knowledge of the magnetoelastic constants and the magnetic layer distortion enables us to calculate the strain-induced magnetocrystalline anisotropy [15]. In the case of tetragonal distortion  $\varepsilon_{11}=\varepsilon_{22}$  and  $\varepsilon_{12}=\varepsilon_{23}=\varepsilon_{13}=0$ . Such distortion induces an additional axial anisotropy perpendicular to the film plane, described by the constant  $K_{si}=b_1(\varepsilon_{11}-\varepsilon_{33})$ , and  $\varepsilon_{33}=-2(c_{12}/c_{11})$  [15]. In Ref. [13] the epitaxial CMG layers of the thicknesses changing from 10 nm to 80 nm deposited also directly on MgO (001) were investigated. The misfit strain was estimated to change from 3.62% for the 10 nm to 2.51% for the 80 nm layer, respectively. If we take  $\varepsilon_{11} \approx 2.5\%$  and the average from our experiments  $b_1 \approx -1 \times 10^7$  erg/cm $^3$ , we obtain  $K_{si} = -5.3 \times 10^5$  erg/cm $^3$ , which is in quite good agreement with the  $K_p$  values presented in Table I. The magnitude of the first cubic magnetocrystalline anisotropy constant of our sample ( $2.2 \times 10^4$  erg/cm $^3$ ) is also very close to the analogous value obtained in Ref. [13] for the 80 nm sample ( $1.9 \times 10^4$  erg/cm $^3$ ). However, an easy axis of magnetization was in our case parallel to [100] direction, and in the case of the sample studied in Ref.[13] - parallel to [110] direction.

The magnetoelastic properties and magnetocrystalline anisotropy of the studied Weyl semimetal CMG thin films are, in many respects, similar to those of the  $\text{Co}_2\text{Fe}_x\text{Mn}_{1-x}\text{Si}$  and  $\text{Co}_2\text{Fe}_{0.4}\text{Mn}_{0.6}\text{Si}$  Heusler alloy thin films, which we investigated in our previous works [14, 15, 20, 21, 22]. All these samples are

\*Contact author: nabia@ifpan.edu.pl

characterized by relatively weak magnetoelastic properties. The magnetoelastic constants ( $b_1$ ,  $b_2$ ) are all negative and on the order of  $10^7$  erg/cm<sup>3</sup>, corresponding to positive longitudinal magnetostriction constants on the order of  $10^{-6}$ . They are also characterized by relatively weak cubic magnetocrystalline anisotropy constants (on the order of  $10^4$  erg/cm<sup>3</sup>) and relatively strong negative perpendicular-to-film magnetocrystalline anisotropy constants (on the order of  $10^5$ - $10^6$  erg/cm<sup>3</sup>).

Our previous studies revealed the influence of magnetic layer thickness on both the magnetoelastic properties and the magnetocrystalline anisotropy constants. Similar effects are likely to be expected for the Weyl semimetal CMG. However, in the present work, all the investigated layers have the same thickness (75 nm). Therefore, we focused on the influence of chemical ordering on magnetocrystalline anisotropy and anisotropic magnetoelastic properties.

For thin films of certain Heusler alloys (such as CMG), achieving a high degree of chemical order may be challenging. In such cases, the degree and type of chemical ordering can significantly affect both the magnetocrystalline anisotropy and the magnetoelastic properties of these layers.

#### IV. CONCLUSIONS

Similarly to other Heusler alloy thin films, epitaxially grown Weyl semimetal CMG thin films exhibit

relatively weak cubic magnetocrystalline anisotropy (MCA) and weak magnetoelastic properties. Increasing the annealing temperature allows for modifications in the chemical ordering of these films, particularly in the proportion of the partially ordered B2 phase and the highly ordered L2<sub>1</sub> phase. Changes in the chemical ordering in epitaxially grown CMG films result in variations in both the MCA and magnetoelastic properties.

The most significant changes in both the cubic MCA and the anisotropy of the magnetoelastic properties are associated with the emergence of the highly ordered L2<sub>1</sub> phase, which appears after annealing at 500°C. This suggests that the development of magnetic Weyl semimetallic features plays a critical role in influencing these magnetic properties. The large out-of-plane axial MCA constant can be attributed to the combined effects of misfit strain and magnetoelasticity.

For Heusler alloy thin films, where achieving a high degree of chemical ordering is challenging, the degree of chemical ordering may serve as a crucial factor in determining their magnetocrystalline anisotropy and magnetoelastic properties.

#### ACKNOWLEDGMENTS

This work was supported by the National Science Centre of Poland, Project No. 2024/53/B/ST7/01848.

- 
- [1] J. Kübler and C. Felser, *Europhys. Lett.* 114, 47005 (2016).
  - [2] K. Manna, Y. Sun, L. MÜchler, J. Kübler, and C. Felser, *Nat. Rev. Mater.* 3, 244 (2018).
  - [3] I. Belopolski et al., *Science* 365, 1278 (2019).
  - [4] Q. Wang, Z. Wen, T. Kubota, T. Seki, and K. Takahashi, *Appl. Phys. Lett.* 115, 252401 (2019).
  - [5] K. Tang et al., *Appl. Phys. Lett.* 118, 062402 (2021).
  - [6] J. Wang et al., *Adv. Electron. Mater.* 8, 2101380 (2022).
  - [7] A. Hirohata et al., *J. Phys. D: Appl. Phys.* 50, 443001 (2017).
  - [8] A. Sakai et al., *Nat. Phys.* 14, 1119 (2018).
  - [9] K. Sumida et al., *Commun. Mater.* 1, 89 (2020).
  - [10] V. A. Oksenenko et al., *J. Magn. Magn. Mater.* 316, e407 (2007).
  - [11] A. Miyashita et al., *J. Appl. Phys.* 130, 225301 (2021).
  - [12] M. J. Pechana, C. Yu, D. Carr, and C. J. Palmström, *J. Magn. Magn. Mater.* 286, 340 (2005).
  - [13] P. Swekis et al., *Nanomaterials* 11, 251 (2021).
  - [14] A. Nabiałek et al., *Phys. Rev. B* 106, 054406 (2022).
  - [15] A. Nabiałek et al., *Sci. Rep.* 13, 17016 (2023).
  - [16] J. C. M. Henning and J. H. den Boef, *Appl. Phys.* 16, 353 (1978).
  - [17] K. Nesteruk et al., *Meas. Sci. Technol.* 25, 075502 (2014).
  - [18] R. Y. Umetsu et al., *Phys. Rev. B* 77, 104422 (2008).
  - [19] R. Amraoui et al., *Eur. Phys. J. B* 95, 198 (2022).
  - [20] O. M. Chumak et al., *IEEE Trans. Magn.* 53, 2501906 (2017).
  - [21] O. M. Chumak et al., *Sci. Rep.* 11, 7608 (2021).
  - [22] A. Nabiałek et al., *IEEE Trans. Magn.* 59, 2501405 (2023).